JOURNAL OF COMPUTATIONAL PHYSICS 3, 339–357 (1969)

A Numerical Model for Linearized Gravity and Acoustic Waves

DAVID D. HOUGHTON AND WALTER L. JONES

National Center for Atmospheric Research, Boulder, Colorado 80302

Received July 15, 1968

ABSTRACT

A numerical model is designed for studying the time-dependent properties of linearized and vertically propagating gravity and acoustic waves in the atmosphere. A finite-difference scheme with second-order accuracy is developed and analyzed for stability and other computational properties. Test computations are made and presented for gravity waves with and without a critical level, and for an acoustic wave. In all three cases the numerical results compare satisfactorily with theoretical results.

I. INTRODUCTION

In a discussion of the critical layer for internal gravity waves in a shear flow, Booker and Bretherton [1] have emphasized the limitations of a steady-state analysis or even an asymptotic-state analysis for gravity waves in the atmosphere. The analytical forms for the time-dependent solutions can be complicated by Laplace transforms [1, 2] and readily subject to solution only in the limit of long time intervals. In addition, further study of internal gravity motions requires extensive consideration of the nonlinear aspects of the problem, e.g., time dependent large-scale motions and energy transfers between different scales of motion. For all of these reasons it was felt important to develop a general numerical model for time-dependent motions of the atmosphere which would be suitable for internal gravity wave and acoustic wave studies.

This paper describes the first version of the model, which encompasses the basic numerical scheme for the linear equations. In a later model, rotation and time-dependent mean flow will be introduced. In the model's fullest form, both perturbation and mean motions will be interlocked, yet separately distinguished, in a nonlinear system.

The success of the model depends not only on an appropriate numerical scheme, but also on a transformation of the original equations which permits formulating the problem with only one space dimension and therefore very high resolution.

581/3/3-1

This is important because we wish to retain accuracy for all of the widely ranging scales of motion that can develop in the model.

In the current linear version of the model, the solutions after a long time can be compared with a wide variety of known linear solutions for steady periodic conditions [3]. Also, for particular cases, comparisons for the acoustic wave solution can be made even after short time intervals. Several comparisons will be made here to demonstrate the great degree of accuracy obtained in the numerical model even after tens of thousands of time steps.

II. Physical Model and Basic Equations

The physical domain modeled is the first 100 km of the atmosphere (Fig. 1). A compressible gas is considered, with all processes being adiabatic. A nonrotating Cartesian coordinate system is used, and the wave perturbations are chosen to vary in the x and z directions. (This is achieved by rotation of the coordinate system about a vertical axis.) A mean wind is taken in the x direction and assumed to be a function of z only. Under these constraints there is no motion in the y direction.

As shown in Fig. 1, an artificial viscous drag, or Rayleigh viscosity, is also introduced into the model. This drag is proportional to perturbation fluid velocity. The proportionality constant is taken to be zero in the height range from $z = 0$,

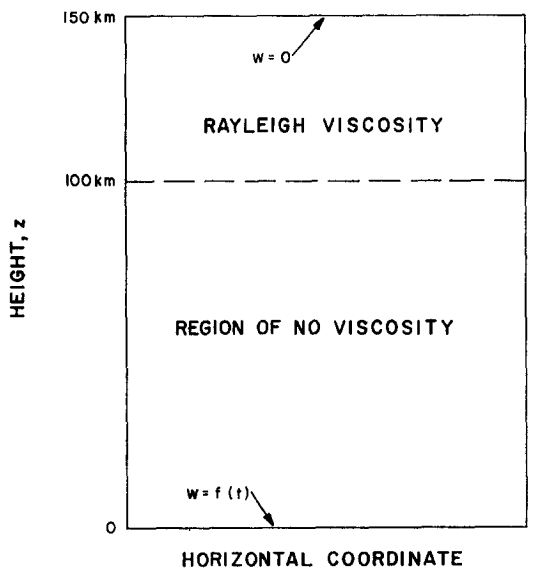

Fig. 1. Physical domain and boundary conditions for the numerical model. All dependent variables are periodic in the horizontal coordinate direction.

the lower boundary, to $z = 100$ km. From $z = 100$ km, the proportionality constant increases more or less exponentially to $z = 150$ km, the upper boundary. The purpose of this artifice is to simulate a "radiation boundary condition" at 100 km, so that waves propagating to this level continue to carry energy to infinity without suffering reflection. The vertical velocity is set equal to zero at 150 km. In practice, waves generated in the lower region are greatly attenuated before reaching this level, and there is negligible reflection.

In general, the initial condition for the operation of the model requires the complete absence of perturbation motion. This helps assure that no waves travel in the wrong direction. Nevertheless, initial nonzero values may be used. The numerical model is constructed so that after the initial time, continuous input of energy is possible at the lower boundary. As will be shown, only w must be prescribed at the lower and upper boundaries. The other variables are completely determined by the finite-difference equations, which will be described in Section III. For the current model, $w = f(t)$ at $z = 0$, and $w = 0$ at $z = 150$ km, where $f(t)$ is arbitrary (see Fig. 1).

The linearized equations for the model include variables which are defined as follows:

c: speed of sound, $\sqrt{\gamma p_0/\rho_0}$
g: acceleration of gravity
K: coefficient of viscosity
p_0: mean pressure
p^*: perturbation pressure
t: time
u_0: mean velocity component in x direction
u^*: perturbation velocity component in x direction
w^*: perturbation velocity component in z direction
x: horizontal coordinate
z: vertical coordinate
γ: ratio of specific heats, $c_p/c_v = 1.4$
ρ_0: mean density
ρ^*: perturbation density

All the mean quantities (u_0, ρ_0, p_0) can be functions of z, but not of x. The quantities p_0 and ρ_0 are related by the hydrostatic condition.

The equations for motion, continuity, and for the first law of thermodynamics are as follows:

for motion,

$$\frac{\partial u^*}{\partial t} + u_0 \frac{\partial u^*}{\partial x} + w^* \frac{du_0}{dz} = -\frac{1}{\rho_0} \frac{\partial p^*}{\partial x} - Ku^* \tag{1a}$$

and

$$\frac{\partial w^*}{\partial t} + u_0 \frac{\partial w^*}{\partial x} = -\frac{1}{\rho_0}\frac{\partial p^*}{\partial z} - \frac{\rho^*}{\rho_0} g - Kw^*; \tag{1b}$$

for continuity,

$$\frac{\partial \rho^*}{\partial t} + u_0 \frac{\partial \rho^*}{\partial x} + w^* \frac{d\rho_0}{dz} = -\rho_0 \left(\frac{\partial u^*}{\partial x} + \frac{\partial w^*}{\partial z}\right); \tag{1c}$$

and for the first law of thermodynamics,

$$\frac{\partial p^*}{\partial t} + u_0 \frac{\partial p^*}{\partial x} - \rho_0 w^* g = -c^2 \rho_0 \left(\frac{\partial u^*}{\partial x} + \frac{\partial w^*}{\partial z}\right). \tag{1d}$$

The basic equations of (1) can be simplified if the horizontal periodicity is accounted for and if ρ_0 is eliminated by a variable transformation. Let

$$\begin{aligned} u^* &= \rho_0^{-1/2} u e^{ikx}, \qquad & w^* &= \rho_0^{-1/2} w e^{ikx}, \\ \rho^* &= \rho_0^{+1/2} \rho e^{ikx}, \qquad & p^* &= \rho_0^{+1/2} p e^{ikx}, \end{aligned} \tag{2}$$

where k is the horizontal wave number. The new variables are analogous to the field variables defined by Eckart [3]. Substituting Eqs. (2) into (1) results in the following equations for these variables:

$$\begin{aligned} \frac{\partial u}{\partial t} &= -iku_0 u - \frac{du_0}{dz} w - ikp - Ku, \\ \frac{\partial w}{\partial t} &= -iku_0 w - \frac{\partial p}{dz} + \frac{\beta}{2} p - g\rho - Kw, \\ \frac{\partial \rho}{\partial t} &= -iku_0 \rho + \frac{\beta}{2} w - iku - \frac{\partial w}{\partial z}, \end{aligned} \tag{3}$$

and

$$\frac{\partial p}{\partial t} = -iku_0 p + \left(g - \frac{c^2\beta}{2}\right) w - c^2 iku - c^2 \frac{\partial w}{\partial z},$$

where

$$\beta = -\frac{1}{\rho_0}\frac{\partial \rho_0}{\partial z},$$

and the dependent variables are now all complex.

Modeling according to Eqs. (3) is far simpler than according to (1). In (3), one dimension is eliminated, and the density-weighted dependent variables tend to be of constant amplitude-range with height for steady conditions, rather than growing

exponentially. In addition, the squares of the amplitudes of the field variables may be related in a simple way to the wave kinetic and potential energies [3].

In the simple case when $u_0 = 0$, $K = 0$, and β, g, and c^2 are constant, Eqs. (3) have well-known solutions [4]. For example, they can then be combined into the form

$$\frac{\partial^4 w}{\partial t^4} - \frac{\partial^4 w}{\partial t^2 \partial z^2} + \left(k^2 c^2 + \frac{\gamma^2 g^2}{4c^2}\right) \frac{\partial^2 w}{\partial t^2} + (\gamma - 1)\, g^2 k^2 w = 0. \tag{4}$$

Solutions can be found with temporal and vertical periodicity of the form

$$e^{-i(k_z z - \omega t)},$$

with the dispersion equation

$$\omega^4 - \omega^2 \left[c^2(k^2 + k_z^2) + \frac{\gamma^2 g^2}{4c^2}\right] + (\gamma - 1)\, g^2 k^2 = 0, \tag{5}$$

where k_z is the vertical wave number.

For given wave numbers, k and k_z, there are two pairs of solutions for ω. The higher frequencies, where $\omega \approx \pm c(k^2 + k_z^2)^{1/2}$ for $\omega \gg \gamma g/2c$, correspond to acoustic waves with upward and downward phase propagation components. The lower frequencies correspond to internal gravity waves, again with opposite signs of vertical phase propagation.

Equations (3) can be written in the form

$$m_t = Am_z + Bm, \tag{6}$$

where

$$m = \begin{pmatrix} u \\ w \\ \rho \\ p \end{pmatrix}, \qquad A = \begin{pmatrix} 0 & 0 & 0 & 0 \\ 0 & 0 & 0 & -1 \\ 0 & -1 & 0 & 0 \\ 0 & -c^2 & 0 & 0 \end{pmatrix},$$

and

$$B = \begin{pmatrix} -iku_0 - K & -du_0/dz & 0 & -ik \\ 0 & -iku_0 - K & \beta/2 & -g \\ -ik & \beta/2 & -iku_0 & 0 \\ -c^2 ik & (g - c^2\beta/2) & 0 & -iku_0 \end{pmatrix}.$$

The classification of the set (6) can be determined by analyzing its characteristics. These are found by setting $\mathrm{Det} \mid A - \lambda_i I \mid = 0$, where λ_i, $i = 1, 4$ represent the characteristic slopes and I is the unit matrix. The four solutions for λ_i are

$$+c, -c, 0, 0.$$

The fact that these solutions are real and represent four linearly independent characteristic vectors indicates that the equations are hyperbolic and suited to solution as an initial and boundary value problem. The first two solutions for λ correspond to the acoustic modes, the last two to the internal gravity wave modes. Since the latter values of λ are zero when we know that internal gravity waves have nonzero vertical phase speeds, it is clear that the undifferentiated or linear terms in (6) are dominant, or at least important, in determining the wave properties.

If Eq. (4) is considered as an initial and boundary value problem, it is well posed if one provides certain conditions. Since the equation is of fourth order in t and second in z, four conditions are placed on w for all z values at specified values of t; also, two conditions are placed on w for all values of t at specified values of z. The orders of the equation are not increased if u_0 and $du_0/dz \neq 0$. Since u, p, and ρ can be specified in terms of w and its derivatives, the first four conditions can be satisfied by specifying these variables and w throughout z at an initial time $t = 0$. The other two conditions are satisfied by specifying $w(t)$ at two particular values of z, the upper and lower boundaries of the model.

III. Finite-Difference System

Because acoustic waves are allowed in this model, we know that the time step will be limited by $\Delta t \leqslant \Delta z/c$, where Δz is the vertical mesh spacing. In order to achieve fine resolution for the slower-moving gravity waves and yet allow them time to develop significantly, it is necessary to have a finite-difference scheme that can apply to very many time steps. For reasonable solutions, therefore, the appropriate scheme should be at least of second order in accuracy and very close to neutral with regard to stability.

It is advantageous to use a staggered grid in space, such that only w is defined on the boundaries. By extending this also to a staggered grid in time, it is a simple matter to construct a finite-difference scheme of second-order accuracy in both time and space. Figure 2 shows the staggered grid employed and the location of the four dependent variables.

For linear equations we know that the "leapfrog" method [5] is neutral for the wave-equation part of (6),

$$m_t = Am_z, \tag{7}$$

as well as of second-order accuracy. When the linear terms are considered, it is not certain *a priori* that a second-order scheme (in time) will also be neutral or close to neutral [6]. However, a scheme centered in all respects except for the viscosity terms seems to be satisfactory. The viscosity terms are lagged half a time-step for numerical simplicity. These terms do not appear in the region of

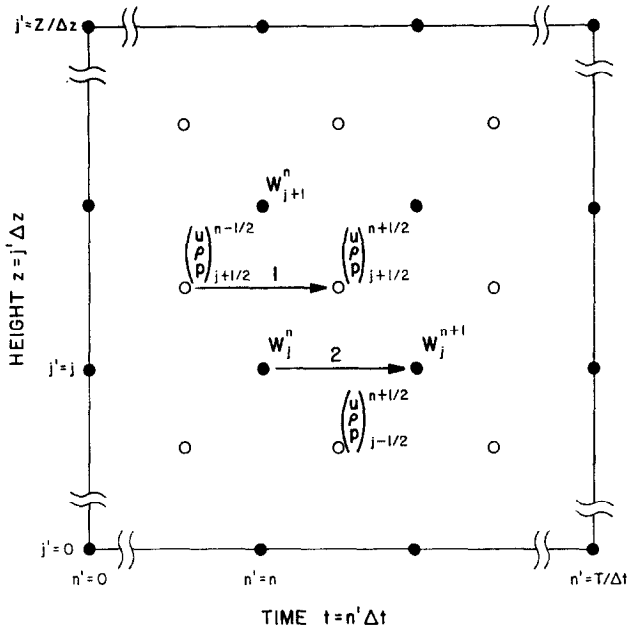

FIG. 2. Basic grid mesh. The variable w is represented by the dots and the variables u, ρ, and p are placed at the circles. Z represents the height of the upper boundary and T the final time. Variables are shown in a cluster corresponding to the finite difference scheme given in the text. The arrows indicate the marching direction, and the numbering indicates the order in which this is done for a given position.

interest, 0 to 100 km. Above 100 km, all that is required is that the finite difference formulation of the viscosity terms dampen the wave motions.

If we make the following definitions

$$r = \begin{pmatrix} u \\ \rho \\ p \end{pmatrix}, \quad R = \begin{pmatrix} 0 \\ -1 \\ -c^2 \end{pmatrix}, \quad S = \begin{pmatrix} 0 & 0 & 0 \\ 0 & 0 & 0 \\ 0 & 0 & -1 \end{pmatrix},$$

$$P = \begin{pmatrix} K & 0 & 0 \\ 0 & 0 & 0 \\ 0 & 0 & 0 \end{pmatrix}, \quad C = \begin{pmatrix} -iku_0 - K & 0 & -ik \\ 0 & -iku_0 & -g \\ -c^2ik & 0 & -iku_0 \end{pmatrix},$$

$$D = \begin{pmatrix} -du_0/dz \\ \beta/2 \\ g - c^2\beta/2 \end{pmatrix}, \quad E = \begin{pmatrix} 0 & 0 & 0 \\ 0 & \beta/2 & 0 \\ 0 & 0 & -g \end{pmatrix},$$

Eq. (6) can be written

$$\begin{aligned} r_t &= Rw_z + Cr + Dw, \\ w_t &= Sr_z + Er - (iku_0 + K)w. \end{aligned} \tag{8}$$

The finite-difference scheme is then represented by

$$r_{j+1/2}^{n+1/2} = (I - \Delta t\, P)\, r_{j+1/2}^{n-1/2} + \frac{\Delta t}{\Delta z} R_{j+1/2}(w_{j+1}^{n} - w_j^{n}) + \frac{\Delta t\, C_{j+1/2}}{2}(r_{j+1/2}^{n+1/2} + r_{j+1/2}^{n-1/2}) + \frac{\Delta t\, D_{j+1/2}}{2}(w_{j+1}^{n} + w_j^{n}), \tag{9a}$$

and

$$w_j^{n+1} = (I - \Delta t\, K)\, w_j^{n} + \frac{\Delta t}{\Delta z} S_j(r_{j+1/2}^{n+1/2} - r_{j-1/2}^{n+1/2}) + \frac{\Delta t\, E_j}{2}(r_{j+1/2}^{n+1/2} + r_{j-1/2}^{n+1/2}) - \frac{\Delta t\, ik(u_0)_j}{2}(w_j^{n+1} + w_j^{n}). \tag{9b}$$

For a given j, these equations must be solved in the sequence (9a) and then (9b) in order to have the necessary values on the right-hand sides at all times (see Fig. 2). The equations can be converted readily into explicit forms. This is done by solving for u using the equations for u and p, and then solving for p, ρ, and w in that order.

IV. Stability Analysis

We apply the von Neumann stability test [7] to the finite-difference equations (9). This is a necessary but not always sufficient condition for numerical stability. Assuming periodic boundary conditions, the dependent variables can be expanded in Fourier series of the form

$$\begin{pmatrix} u \\ \rho \\ p \\ w \end{pmatrix} = \sum_{\alpha=0}^{\pi/\Delta z} \begin{pmatrix} \bar{u}(t, \alpha) \\ \bar{\rho}(t, \alpha) \\ \bar{p}(t, \alpha) \\ \bar{w}(t, \alpha) \end{pmatrix} e^{i\alpha j \Delta z}, \tag{10}$$

where α is the wave number in the z direction. Then, by assuming constant coefficients for the linear finite-difference equations, (10) can be substituted into (9a, b) to result in an independent set of equations for each Fourier component amplitude: $\bar{u}$, $\bar{\rho}$, $\bar{p}$, and $\bar{w}$. If $\theta = \alpha \Delta z/2$, these equations can be written

$$Y\bar{m}^{n+1/2} = X\bar{m}^{n-1/2}, \tag{11}$$

where

$$\bar{m}^{n+1/2} = \begin{pmatrix} \bar{u}^{n+1/2} \\ \bar{\rho}^{n+1/2} \\ \bar{p}^{n+1/2} \\ \bar{w}^{n+1} \end{pmatrix}, \qquad \bar{m}^{n-1/2} = \begin{pmatrix} \bar{u}^{n-1/2} \\ \bar{\rho}^{n-1/2} \\ \bar{p}^{n-1/2} \\ \bar{w}^{n} \end{pmatrix},$$

$$Y = \begin{bmatrix} 1 + \frac{iku_0\Delta t}{2} & 0 & \frac{ik\Delta t}{2} & \frac{\Delta t}{2}\frac{du_0}{dz} \\ \frac{ik\Delta t}{2} & 1 + \frac{iku_0\Delta t}{2} & 0 & 0 \\ \frac{ik\Delta tc^2}{2} & 0 & 1 + \frac{iku_0\Delta t}{2} & 0 \\ 0 & g\Delta t\cos\theta & \Delta t\left(\frac{2i\sin\theta}{\Delta z} - \frac{\beta}{2}\cos\theta\right) & 1 + \frac{iku_0\Delta t}{2} \end{bmatrix},$$

and

$$X = \begin{bmatrix} 1 - \frac{iku_0\Delta t}{2} - K & 0 & -\frac{ik\Delta t}{2} & -\frac{\Delta t}{2}\frac{du_0}{dz} \\ -\frac{ik\Delta t}{2} & 1 - \frac{iku_0\Delta t}{2} & 0 & -\Delta t\left(\frac{2i\sin\theta}{\Delta z} - \frac{\beta}{2}\cos\theta\right) \\ -\frac{ik\Delta tc^2}{2} & 0 & 1 - \frac{iku_0\Delta t}{2} & \Delta t\left[\left(g - \frac{c^2\beta}{2}\right)\cos\theta - \frac{2ic^2\sin\theta}{\Delta z}\right] \\ 0 & 0 & 0 & 1 - \frac{iku_0\Delta t}{2} - K \end{bmatrix}.$$

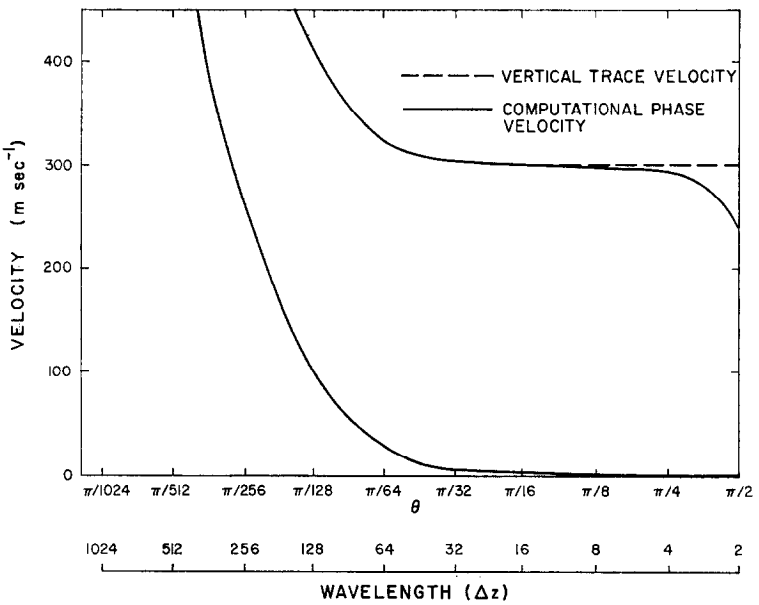

FIG. 3. Vertical trace velocity and computational phase velocities for the two upward moving modes as a function of wavelength, shown in terms of θ and the number of grids per wavelength, There is no mean wind.

Equation (11) can also be written in the form

$$\bar{m}^{n+1/2} = G\bar{m}^{n-1/2}, \tag{12}$$

where G, the amplification matrix, is given by

$$G = Y^{-1}X.$$

A necessary condition for stability is that the maximum absolute value of the four eigenvalues of G be bounded by $1 + M\Delta t$, where M is a constant. Numerical determination of the eigenvalues showed that their maximum absolute value was bounded by $1 + M\Delta t$ when the Courant–Friedricks–Lewy condition, $\Delta t \leqslant \Delta z/c$, was satisfied and the viscosity coefficient was reasonably small.

Since the numerical scheme is for very many time steps, it must be not only stable but also very accurate. The accuracy of the scheme can be evaluated by examining the magnitudes and phase angles of the eigenvalues for matrix G. If $du_0/dz = 0$ and $K = 0$, then the magnitudes of the four eigenvalues of G are all identically unity, implying a neutral scheme. The phase angles can be converted to computational phase velocities. These are shown in Fig. 3 for the two upward-

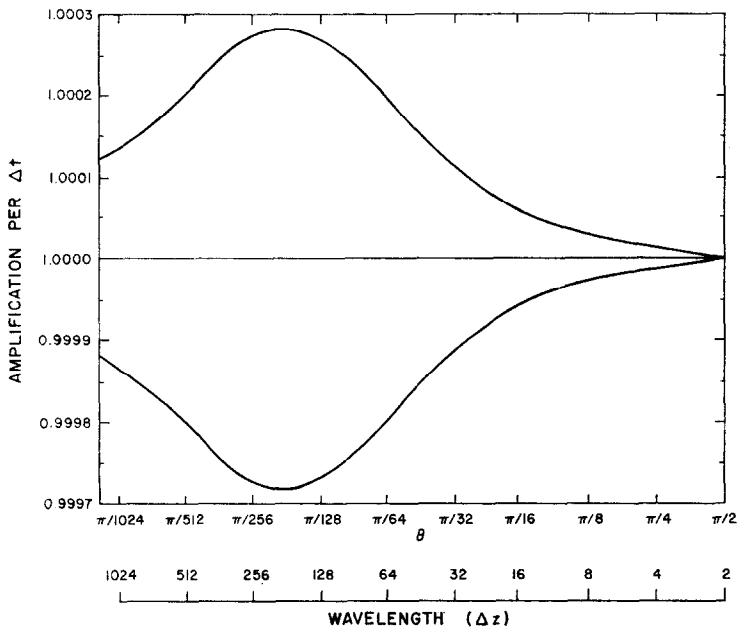

FIG. 4. Maximum and minimum amplitudes for eigenvalues for a mean wind shear of -10^{-3} sec^{-1} and a mean wind of -50 m sec^{-1} as a function of vertical wavelength.

moving modes of the case $du_0/dz = 0$. (For each upward mode, there is an equal but opposite downward-moving mode.)

In Fig. 3, the computational phase velocity is shown by the unbroken line, and the vertical trace velocity, computed from the physical dispersion relationship of Eq. (5), is shown by the dashed line. For most values of θ, the vertical trace velocity agrees so closely with the computational phase velocity that it cannot be indicated graphically in Fig. 3. However, for the acoustic mode, at very short wavelengths, the computational phase velocity becomes significantly less than the trace velocity.

If a velocity shear du_0/dz is introduced, the eigenvalue magnitudes are no longer identically unity, but they show slight damping and amplification. Figure 4 shows the maximum and minimum magnitudes for $du_0/dz = -10^{-3}\ \text{sec}^{-1}$ and $u_0 = -50\ m\ \text{sec}^{-1}$, with other parameters set equal to geophysical values to be described later. The largest and smallest magnitudes occur for a very large wavelength, about $150\ \Delta z$, and the greatest change indicated is $\pm 0.03\,\%$ per time step.

If $du_0/dz = 0$ and a small viscous damping is present ($K \neq 0$), analysis of G indicates that all of the wave modes are damped for all values of θ except for one at the shortest possible wavelength, $\theta = \pi/2$, which remains identically neutral.

V. Test Cases

In each of three test cases, a theoretical solution for the time-dependent or asymptotic time-dependent motions is compared with the numerical results. An isothermal atmosphere is assumed (Laplacian speed of sound, $c = 300\ \text{m sec}^{-1}$). For each case, the coefficient of damping is prescribed as follows:

For $z < z_0$,

$$K = 0,$$

and for $z \geqslant z_0$,

$$K = K'[e^{(z-z_0)/L} - 1],$$

where K' is a constant, z_0 is 100 km, and L (defining the vertical scaling) is set equal to 15 km. In the first test case the maximum $K\Delta t$ is 0.10; in the other two it is 0.05. The vertical grid spacing is 250 m, i.e., there are 600 grid points with 200 in the upper damping region. The time step is 3/4 sec.

Case A: Acoustic Wave

An acoustic wave is produced with no horizontal variations, $k = 0$, and with a non-periodic forcing at the lower boundary: $w = 1$, $t \geqslant 0$. The theoretical solution [8] is given by

$$w = w_0 \left\{ 1 - \frac{z}{2H} \int_{z/c}^{t} \frac{J_1\left[\frac{c}{2H}\sqrt{\nu^2 - (z/c)^2}\right]}{\sqrt{\nu^2 - (z/c)^2}}\, d\nu \right\}, \tag{13}$$

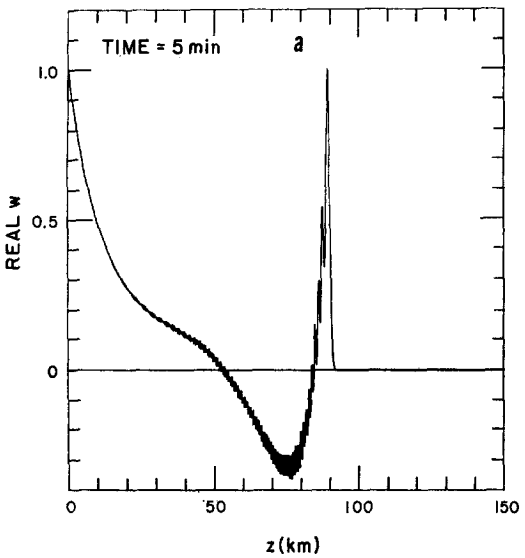

FIG. 5a. Numerical solution for real w after 5 min, where $k = 0$ and $w(0, t) = 1$.

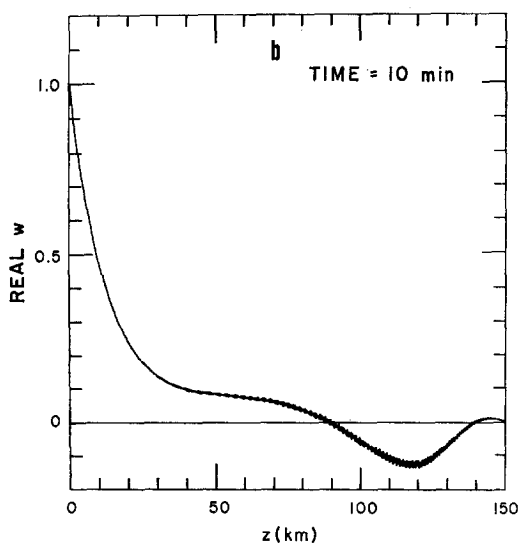

FIG. 5b. Same as Fig. 5a but after 10 min.

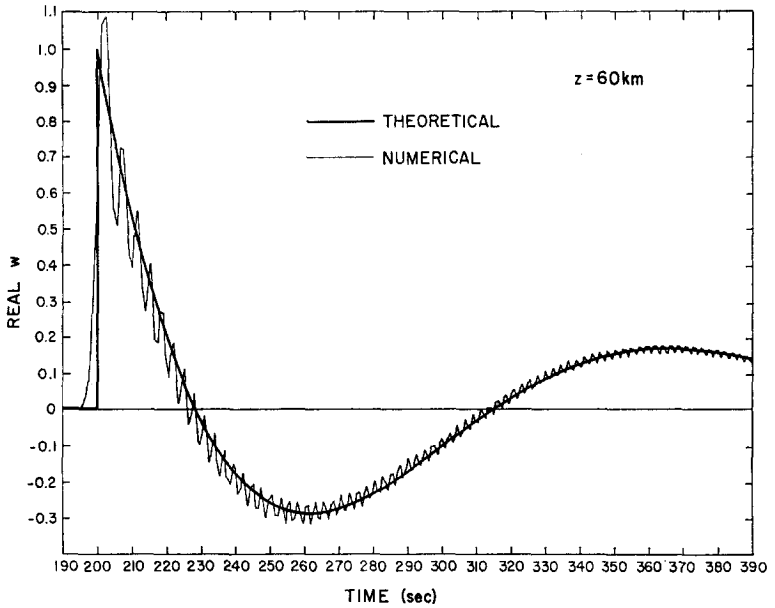

FIG. 6. Comparison of theoretical and numerical solutions as a function of time at 60 km, with $k = 0$ and $w(0, t) = 1$.

where H is the scale depth equal to $c^2/\gamma g$, J_1 is the Bessel function of the first order, and ν is a dummy variable for time.

Calculations were made for 20 min of real time, or 1600 time steps. This took 3 min on the Control Data 6600 computer. Figures 5a and 5b show the numerical solutions for w at 5 and 10 min, respectively. In the latter case, the damping effects above 100 km are quite evident. Figure 6 shows the comparison for w at the 60-km level between the numerical computation and the theoretical solution given by Eq. (13).

Case B: Gravity Wave with No Mean Wind

A steady forcing at the lower boundary corresponds to a horizontal wavelength of 100 km ($k = 2\pi \times 10^{-5}$) and a period of 30 min with no mean motions. The forcing function, smoothed for the first part of the calculation to reduce sound-wave production, is given by

$$w(0, t) = (1 - e^{(\omega/2)t})\, e^{i\omega t}, \tag{14}$$

where $\omega = 3.4907 \times 10^{-3}$ sec^{-1}.

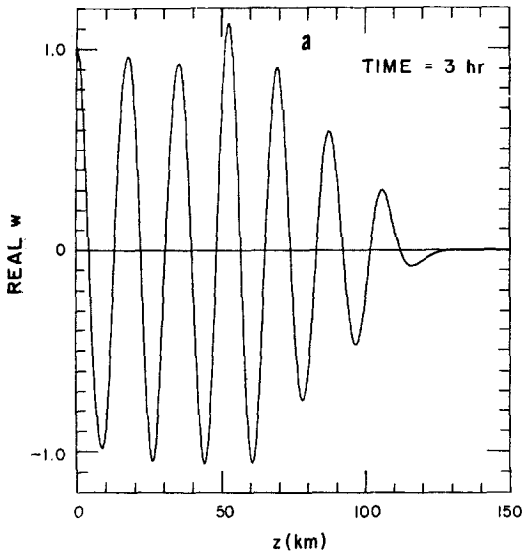

FIG. 7a. Numerical solution for real w after 3 h, with $k = 6.2832 \times 10^{-5}$, $\omega = 3.4907 \times 10^{-3}$, and $w(0, t) = (1 - e^{(\omega/2)t})\, e^{i\omega t}$. There is no mean wind. Units are mks.

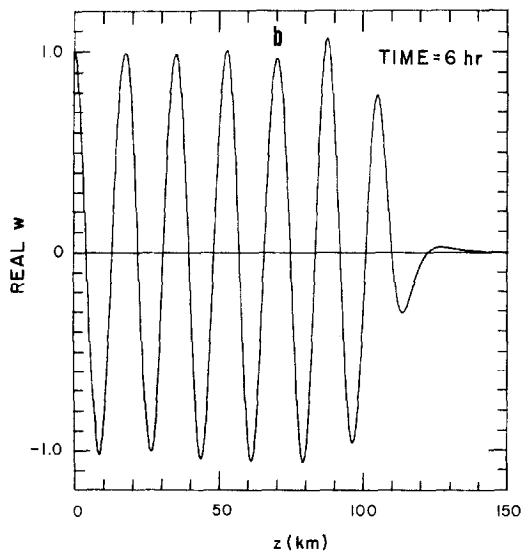

FIG. 7b. Same as Fig. 7a but after 6 h.

After a long time, the asymptotic solution is expected to approach the state described by the dispersion relationship of Eq. (5). With the given k, c, and ω, and with $g = 9.8\ \text{m sec}^{-1}$ and $\gamma = 1.4$, Eq. (5) yields $k_z = \pm 3.5871 \times 10^{-4}$. This gives a vertical wavelength of 17.516 km and a vertical trace velocity of $\pm 9.731\ \text{m sec}^{-1}$.

The question remains as to how long it should take to reach the asymptotic solution throughout the physical region, 0 to 100 km. This can be estimated by computing the group velocity from the dispersion relationship (5), which gives

$$c_g = \frac{\omega c^2 k_z}{2\omega^2 - c^2(k^2 + k_z^2) - \gamma^2 g^2/4c^2}. \tag{15}$$

For the parameters in this experiment, $c_g = \mp 9.063\ \text{m sec}^{-1}$. The difference in signs means that the phase and group velocities are opposite. Since the energy is input at the lower boundary, only the modes with upward moving group velocity and downward moving phase velocity should be present. Furthermore, the group velocity indicates that it should take at least three hours for the steady oscillatory conditions to be established up to 100 km.

Computations were made for 6 h of real time, and required 1 h on the Control Data 6600 computer. Figures 7a and 7b show the real w field after 3 and 6 h, respectively. In Fig. 8, the near-asymptotic conditions existing after 6 h are shown by the approximate constancy of the product real uw' with height, where w' is the

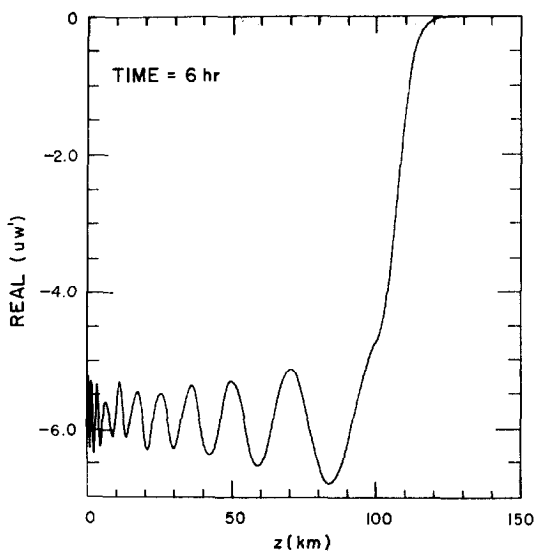

FIG. 8. The product real (uw') where w' is the complex conjugate of w for the numerical experiment described in Fig. 7a after 6 h.

complex conjugate of w. The vertical momentum transport is equal to one-half the magnitude of real uw'. The vertical wavelength determined from Fig. 7b is 17.5 km, which agrees favorably with theory. Other oscillation modes created by the sudden start-up of w are still present as some of them have very small group velocities. The results of computations in motion picture form from CRT output show dramatically the downward phase velocity, together with an upward group velocity.

Case C: Gravity Wave with Mean Wind Shear and a Critical Level

Booker and Bretherton [1, 9] have discussed the effect of a critical level due to mean wind shear on the gravity wave. At this level, where the horizontal phase velocity of the wave equations equals the mean fluid velocity, a singularity occurs in the equations for waves with a steady state periodic oscillation. Bretherton has analyzed this problem in terms of the WKB approximation and concluded that a wave packet approaches this level asymptotically with ever-decreasing group velocity. In the steady-state solution, the vertical wavelength and vertical velocity vary as the square root of the distance to the critical level, while the horizontal velocity varies as the inverse square root of this distance. Also, the vertical momentum flux is constant below and above the critical level, but discontinuous across it.

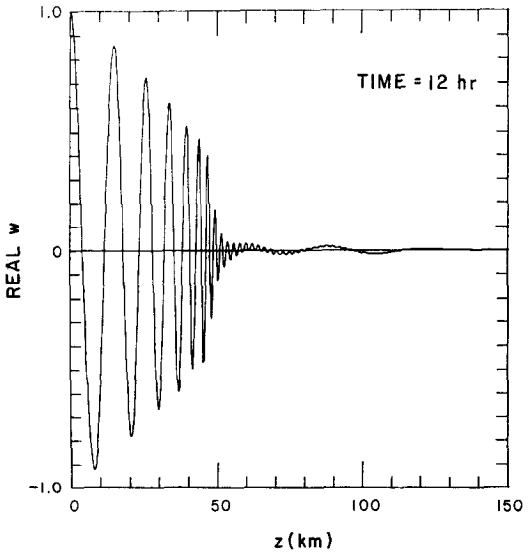

FIG. 9. Numerical solution for real w after 12 h, with $k = 6.2832 \times 10^{-5}$, $\omega = 3.4907 \times 10^{-3}$, and $w(0, t) = (1 - e^{(\omega/2)t})\, e^{i\omega t}$. Mean wind is given by $-10^{-5}z$ m sec^{-1} when $0 \leqslant z \leqslant 10^5$ m, and by -100 m sec^{-1} when $z > 10^5$ m. Units are mks.

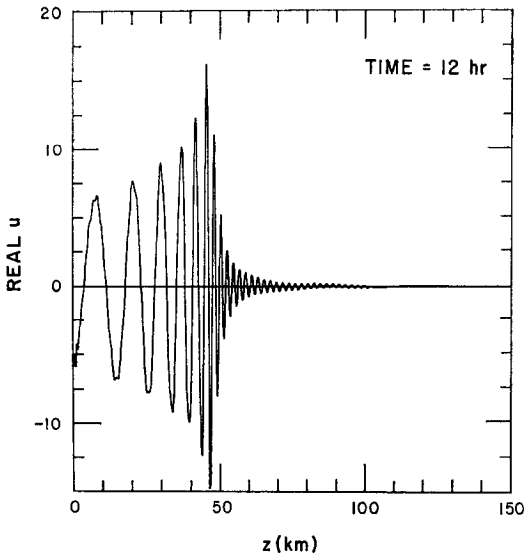

FIG. 10. Numerical solution for real u after 12 h for the model parameters given in Fig. 9.

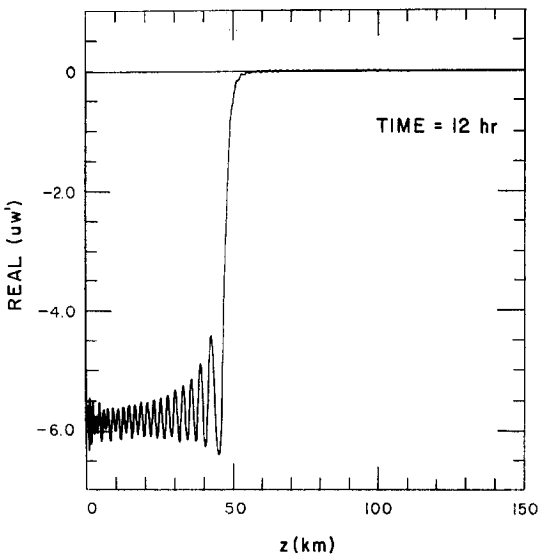

FIG. 11. The product real (uw') after 12 h for the experiment described in Fig. 9.

A numerical calculation was tried with $u_0 = -10^{-3} z$ m sec^{-1} and $du_0/dz = -10^{-3}$ sec^{-1} up to 100 km, and then with $u_0 = -100$ m sec^{-1} above 100 km in the damping layer. With the same period and horizontal wavelength as used before, the horizontal phase speed was found to be 56.6 m sec^{-1}. Therefore, the critical level in this model is at 56.6 km. Calculations were run for 12 h. Figures 9, 10, and 11 show the real w, u, and uw' fields after 12 h. All of the behavior expected theoretically is demonstrated.

If the calculation is continued, the vertical wavelength approaches the smallest resolvable ($2\Delta z$) and truncation effects become noticeable. The u magnitudes do not continue to grow indefinitely but level off. This damping agrees with the analysis of the amplification matrix eigenvalues for mean wind conditions, which are approximately equal to those at the critical level. The solutions for the eigenvalues indicate that the two fast-moving modes (acoustic waves) amplify slightly and the two slow-moving modes (gravity waves) are both slightly damped.

VI. Conclusions

The numerical model described is shown to give rather accurate solutions for both accoustic and gravity wave motions. Accuracy is determined by comparing numerical results with theoretical solutions for asymptotic limits in the case of gravity waves, and with a particular time dependent solution in the case of acoustic waves.

The model can have slow amplification of wave modes, but these do not seem to introduce large nonphysical errors. Calculations here show up to 57,600 time steps. Even in tests involving up to 115,200 time steps, the solutions show great accuracy. Of course, at critical levels, accuracy is gradually lost, but this problem is of local extent and is significant only after a long time.

The viscous zone between 100 km and the upper boundary at 150 km provides a very good approximation to a radiation condition at 100 km. The reflected wave energy from the upper region is insignificant even for the fast-moving sound waves.

Acknowledgments

The authors wish to thank Dr. J. Gary and Dr. A. Kasahara for reviewing the manuscript.

References

1. J. R. Booker and F. P. Bretherton, *J. Fluid Mech.* **27**, 513 (1967).
2. R. E. Dickinson, Propagators of Atmospheric Motions [M.I.T., Department of Meteorology, Planetary Circulations Project, Report No. 18 (1966)].

3. C. ECKART, "Hydrodynamics of Oceans and Atmospheres." Pergamon Press, New York (1960).
4. C. O. HINES, *Canadian J. Phys.* **38**, 1441 (1960).
5. R. D. RICHTMYER, A Survey of Difference Methods for Non-Steady Fluid Dynamics [National Center for Atmospheric Research, Technical Note 63-2 (1963)].
6. D. WILLIAMSON, *J. Computational Phys.* **1**, 51 (1966).
7. E. ISAACSON and H. B. KELLER, "Analyses of Numerical Methods." Wiley, New York (1966).
8. H. U. SCHMIDT and J. B. ZIRKER, *Astrophys. J.* **138**, 1310 (1963).
9. F. P. BRETHERTON, *Quart. J. Roy. Meteorol. Soc.* **92**, 466 (1966).